Applied Catalysis B: Environmental 306 (2022) 121135

Contents lists available at ScienceDirect

Applied Catalysis B: Environmental

journal homepage: www.elsevier.com/locate/apcatb

High-performance electroreduction CO_2 to formate at Bi/Nafion interface

Sheng Chang [a], Yimin Xuan [a,*], Jingjing Duan [b], Kai Zhang [a]

[a] School of Energy and Power Engineering, Nanjing University of Aeronautics and Astronautics, Nanjing, Jiangsu 210016, China
[b] School of Energy and Power Engineering, Nanjing University of Science and Technology, Nanjing, Jiangsu 210094, China

ARTICLE INFO

Keywords:
CO_2 reduction
Nafion
Bismuth
Formate
Interface

ABSTRACT

Electrochemical CO_2 conversion into valuable products provides a promising solution for achieving a carbon-neutral energy cycle. Herein, an active and stable Bi/Nafion interface is fabricated over Bi nanosheets with the modification of Nafion, which exhibits superior CO_2 conversion with formate selectivity of above 95% in a wide potential range, partial current density of 72.12 mA cm^{-2} at − 1.07 V *vs.* RHE in H-type cell. The extraordinary CO_2 reduction performance could be ascribed to a high CO_2 permeability and enhanced local proton activity at the Bi/Nafion interface, which leads to promoted CO_2 adsorption and feasible proton-coupled electron transfer during the CO_2 reduction process. Computational investigations reveal the modification of Nafion offers a comfortable platform to enable the key intermediate *OCHO to be stable. This work offers a valuable insight into interfacial manipulation of electrodes to convert CO_2 to valuable products.

1. Introduction

Electrochemical CO_2 reduction reaction (CO_2RR) is an ideal route to achieve carbon-neutral energy cycle [1–6] and the CO_2RR can produce a variety of valued product, such as CO [7,8], CH_4 [9–12], formate [13–15], CH_3OH [16], C_2H_4 [17,18], and so on. Among these products, formate is of great potential for energy chemical manufacturing [19–23] due to its feasible 2-electron thermodynamic process [4] and high economic benefits [24]. Nevertheless, it remains a great challenge to develop CO_2RR catalysts or systems toward formate production with industrial practicability, including high product selectivity, low overpotential and, satisfactory durability [25–27].

Therefore, tremendous efforts have been devoted to catalysts design, where Bi-based catalysts have been extensively studied owing to their strong adsorption of CO_2 intermediates and poor HER activity [25,28,29]. Many strategies have been employed to improve catalysts' intrinsic catalytic activities, such as nano-structuralization [27,30–32], facet or grain engineering [33], electrode surface activation [34], modulation of electron density [35], single atomization [36], vacancy/doping engineering [37–39] and alloying [40–43]. However, limited CO_2 mass transfer and sluggish proton migration usually result in an imbalance of local CO_2/H^+ supply at the vicinity of the electrode surface, which leads to sluggish CO_2RR reaction kinetics and favored HER [44].

The local interface environment at the electrode surface plays an essential role in the CO_2RR process [44,45]. The interface could manipulate the solid/liquid/gas contact, mediate transport and local concentration of reacting species and products, thereby influencing the electrochemical process [46]. The activity and selectivity of the CO_2RR can be modified further by introducing a stable, active interface by using organic molecules like polymers. For example, an artificial electrode/electrolyte interface with a quaternary ammonium cation (R_4N^+) surfactant has been developed, which leads to enhanced formate selectivity due to the stabilization of a key intermediate, OCHO* , through interaction with R_4N^+ [44]. Creation of a nitrogen doped carbon layer over Cu was reported to improve the selectivity of C_{2+} products, which not only enriches and activates CO_2 molecules through N-CO_2 interaction but also protects Cu catalysts from collapse [47]. These studies demonstrate that a stable interface requires a balance between reactive gas and liquid electrolytes [48], which can facilitate the mass transport of CO_2 and prevent electrolyte flooding [49].

Here, we fabricated a stable, active Bi/Nafion interface in contact with electrolytes over Bi-based catalysts, which leads to superior performance for CO_2RR to formate. In detail, the electrode was prepared by modifying Bi nanosheets (Bi NSs) with a Nafion solution *via* a facile physical deposition protocol. The as-resultant electrode exhibits a remarkably high yield of formate with a maximum faradaic efficiency of 97.3% over a wide potential range, and a partial current density of 72.12 mA cm^{-2} at − 1.07 V *vs.* RHE. To the best of our knowledge, it is one of the highest CO_2RR performance to formate production in H-cells among reported Bi-based catalysts. Such a great improvement could be

* Corresponding author.
E-mail address: ymxuan@nuaa.edu.cn (Y. Xuan).

https://doi.org/10.1016/j.apcatb.2022.121135
Received 13 November 2021; Received in revised form 18 January 2022; Accepted 21 January 2022
Available online 25 January 2022
0926-3373/© 2022 Elsevier B.V. All rights reserved.

ascribed to the durable, efficient Bi/Nafion interface, which accelerates the CO_2 adsorption and absorption, promotes the local proton activity at the vicinity of the electrode surface, and protects catalysts from deactivation due to Nafion as a protective layer.

2. Experimental section

2.1. Materials

All chemicals are analytic grade and used without further purification. Bismuth nitrate pentahydrate ($Bi(NO_3)_3$ 5 H_2O), Nafion-117 (5%) solution, poly(vinylidene fluoride) (PVDF), Potassium bicarbonate ($KHCO_3$) were purchased from Aladdin Industrial Corporation. Hydrochloric acid (HCl), acetone, and potassium hydroxide (KOH) were purchased by Sinopharm Chemical Reagent Co. Ltd, China. The pristine Copper foam, Nickel foam as electrode substrates were purchased from Material Technology Co. Ltd, Wuhu, China. The purchased electrode substrate was cut into a 1 × 2 cm^2 area and washed ultrasonically in acetone, 1 M HCl, and deionized (DI) water for 30 min sequentially to remove oxides and oils from the surface, and then dried in a stream of nitrogen for later use. All water used in experiments is DI water.

2.2. Synthesis of Bi bulks@Cu foam

Electrodeposition is a preferred synthesis method based on its wide availability, material flexibility, and cost-effectiveness [50]. The Bi bulks@Cu foam was prepared on copper foam substrate by electrodeposit as follows: firstly, an aqueous precursor electrolyte consisted of 0.05 M $Bi(NO_3)_3$ 5 H_2O and 1.5 M HCl. Cu foam was immersed in the precursor electrolyte as the working electrode, while an Ag/AgCl and a graphite rob were used as reference electrode and counter electrode, respectively. Before the electrodeposition takes place, the working electrode was kept in the precursor electrolyte for 60 s to allow sufficient ion exchange on the electrode surface. The electrodeposition was conducted by applying − 0.8 V *vs*. Ag/AgCl for 30 s, and the deposition solution was stirring at 850 rpms. In the same way, pure nickel foam also was employed as substrate as working electrode as a comparison. Finally, all of the electrodes were obtained by the mentioned way were rinsed several times with deionized water, and dried in a vacuum oven at 60 ℃ overnight.

2.3. Synthesis of Bi NSs@Cu foam by In situ electrochemical reduction

The Bi NSs@Cu foam was obtained by facile *in situ* electrochemical reduction of as-prepared Bi bulks@Cu foam. *In situ* electrochemical reduction was conducted in CO_2-saturated 0.5 M $KHCO_3$ electrolyte with an applied potential of − 0.8 V *vs.* Ag/AgCl for 20 min, then were rinsed several times with deionized water and dried in a vacuum oven at 60 ℃ overnight.

2.4. Synthesis of Naf/Bi NSs@Cu foam

The Naf/Bi NSs@Cu foam was prepared by a simple impregnation method with precursors: Nafion 117, ethanol solutions in the amount of 40 *u*L and 1 mL, respectively. The previously prepared Bi NSs@Cu foam was immersed in the precursor for 60 s and then taken out and dried in a vacuum drying oven overnight. Other electrodes were prepared in the same way. As a comparison, PVDF was used as an alternative of Nafion, was modified by drop-casting 50 *u*L of PVDF/DMF (5 mg mL^{-1}) solution onto the electrode or substrate.

2.5. Characterization

The morphology and microstructure of the as-prepared electrode were investigated *via* field emission scanning electron microscopy (SEM, GeminiSEM 300, Germany) at an acceleration voltage of 2 kV and transmission electron microscopy (TEM, JEM-2100 F, JEOL, Japan) at an acceleration voltage of 200 kV. The crystal phase of the samples was characterized *via* X-ray diffraction (XRD, Bruker D8 ADVANCE, Germany) using Cu Kα. radiation at a scanning rate of 2° min^{-1} in the 2θ from 20° to 80° and the operating current and voltage were 40 kV and 40 mA, respectively. The X-ray photoelectron spectroscopy (XPS) measurements were carried out by PHI 5000 (VersaProbe, Japan). The samples were irradiated with monochromatic Al-Kα radiation. Survey scans were performed using a step size of 0.25 eV/step. The water contact angle was measured by the sessile drop method using FTA1000 contact angle system (First Ten Angstroms, Inc.) at room temperature.

2.6. Electrochemical measurements

All the electrochemical measurements of CO_2 reduction were performed in a typical H-type cell where the anodic and cathodic compartments were separated by Nafion 117 membranes to prevent the reoxidation of CO_2 reduction product. All of the tests were controlled by an electrochemical workstation (CHI 760E, CH Instruments, Inc., USA), equipped with a three-electrode system. A Pt foil and an Ag/AgCl were used as the counter electrode and reference electrode, respectively. CO_2-saturated 0.5 M $KHCO_3$ solution was used as the electrolyte, which was stirred at a rate of 850 rpm during electrolysis and the flow rate of CO_2 was kept at 20 sccm throughout the test process. The prepared electrodes were used as a working electrode with an effective area of 1 cm^2. The potential measured against Ag/AgCl was convent to the reversible hydrogen electrode (RHE) using the following formula: E (*vs.* RHE) = E (*vs.* Ag/AgCl) + 0.197 V + 0.0591 × pH.

After each bulk electrolysis at a constant potential, gaseous products were quantified by an Agilent Technologies gas chromatography system equipped by a thermal conductivity detector (TCD) and flame ionization detector (FID). The liquid products were tested by Bruker AVIII 500 MHz NMR spectroscopy. Typically, in the 1 H NMR analyses, 500 *u*L of collected electrolyte from cathodic compartment was mixed with 100 *u*L D_2O and 10 *u*L DMSO where D_2O was used as a deuterium source and DMSO as an internal standard.

In situ Raman tests were concluded by Raman spectrometer equipped with 532 nm light in a home-built H-type electrolytic cell.

The faradic efficiency (FE) of different products were calculated as follows:

$$FE = \frac{zFN}{It}$$

where z is the number of transfer electrons, which is 2, 2, and 2 for H_2, CO, and HCOOH, respectively. F is the faraday constant (96485 C mol^{-1}). N is the moles of products, according to the standard curves line of GC and 1 H NMR. I, is the test current, received from the average electrocatalysis current during a fixed time (t) and t is the reaction time of CO_2 reduction reaction process.

The cathode energy efficiency was calculated to define the energy utilization toward the formate product using the following equation:

$$EE = \frac{1.23\text{-}E_{formate}}{1.23\text{-}E} \times FE_{formate} \times 100\%$$

where $E_{formate}$ of − 0.199 V *vs.* RHE is the thermodynamic potential for formate formation, 1.23 V is the standard potential for the oxygen evolution reaction and E is the applied potential of *vs.* RHE.

2.7. Computations

All theoretical calculations were performed by using the density functional theory (DFT) method with pseudo-potential plane-wave, which was executed on VASP. The Perdew-Burke-Ernzerbof (PBE) accompanies with generalized gradient approximation (GGA) was utilized to record Exchange-Correlation Specific functionals [51]. All of the

Kohn-Sham wave functions were obtained *via* setting plane wave energy cutoff of 400 eV. The gaussian integration scheme was applied to electron occupancy with an energy smearing width of 0.5 eV. The K-mesh in Brillouim Zone for Self-consistent calculation (SCF) was employed using a 1 * 1 * 1 gamma point mesh [52]. The electron relaxation (convergence with 1.0 $*10^{-5}$ eV/atom) and force (convergence with 0.05 eV/Å) were taken as the criterion during structure optimizations. The spin polarization was included in all of the simulations.

The rhombohedral Bi (003) plane was adapted as the computational model with a 4 * 8 supercell for geometry optimization because of its one of the most stable planes in Bi single crystal [53]. A 12 Å vacuum layer was set along the c-direction in case of interaction between adjacent unit cells. The Gibbs free energy changes (ΔG) of each electrochemical reaction was calculated by $\Delta G = \Delta E + \Delta EZPE - T\Delta S$ (where ΔE is the total electronic energy change, ΔEZPE and ΔS are change of Zero-point energy correction and entropy, respectively. All of the above energy was calculated from DFT simulations. T is the reaction temperature.).

3. Results and discussion

3.1. Preparation and structure characterization

As shown in Fig. 1a, the Bi electrode surface was modified by Nafion through a facile physical deposition method. (See the Supporting information for detailed experimental methods). Cu foam (Fig. S1) was chosen as an electrode substrate because of its high surface area and three-dimensional porous structure that are beneficial for mass transport and active site exposure [28]. Typically, Bi NSs@Cu foam was synthesized *via* feasible electro-deposition protocol (Fig. 1b, Bi bulks@Cu foam) followed by *in situ* treatment of electrochemical reduction (Fig. S2, Fig. 1c). The Bi NSs exhibited a petal-like morphology with a thickness of ~52 nm. The existence of Bi NSs was further evidenced by XPS (Fig. S3).

Then Nafion solution was impregnated into the porous framework of Cu foam and presented on Bi NSs (Naf/Bi NSs@Cu foam) which was verified by XPS (Fig. S4, Fig. S5). The symmetrical F 1 s peak at 689.2 eV are characteristic peaks of Nafion [54], which still presented after a 10-hour CO_2RR process (Fig. S5-6) suggesting Nafion is stable on the Bi NSs electrode during the electrochemical process. SEM and energy-dispersive X-ray spectroscopy (EDS) analysis were employed to assess the uniformity of Nafion on the electrode surface. Fig. 1d showed that Naf/Bi NSs@Cu foam also presented a petal-like structure, indicating the Nafion modification did not damage the structure of Bi NS. The EDS of Bi and F elements indicates that Nafion is homogeneously distributed on the Bi NSs matrix. (Fig. S7). TEM (Fig. 1d-e) further confirmed the existence of Bi crystals with a lattice spacing of 0.33 nm corresponding to (012) planes of metallic Bi (Fig. 1e). EDS from TEM (Fig. 1f) further proved the uniform distribution of Nafion on the Bi NSs@Cu foam surface, with a F/Bi atomic ratio of ~42.2% (Fig. S8). XRD patterns (Fig. 1g) indicated that the modification of Nafion does not affect the crystal structure of Bi NSs, all samples with characteristic diffraction peaks of metallic Bi (Standard PDF card: #85–1329).

3.2. Performance of CO_2RR

The CO_2RR performance of as-prepared electrodes was evaluated between the potential range of − 0.67 and − 1.17 V *vs.* RHE in a CO_2-

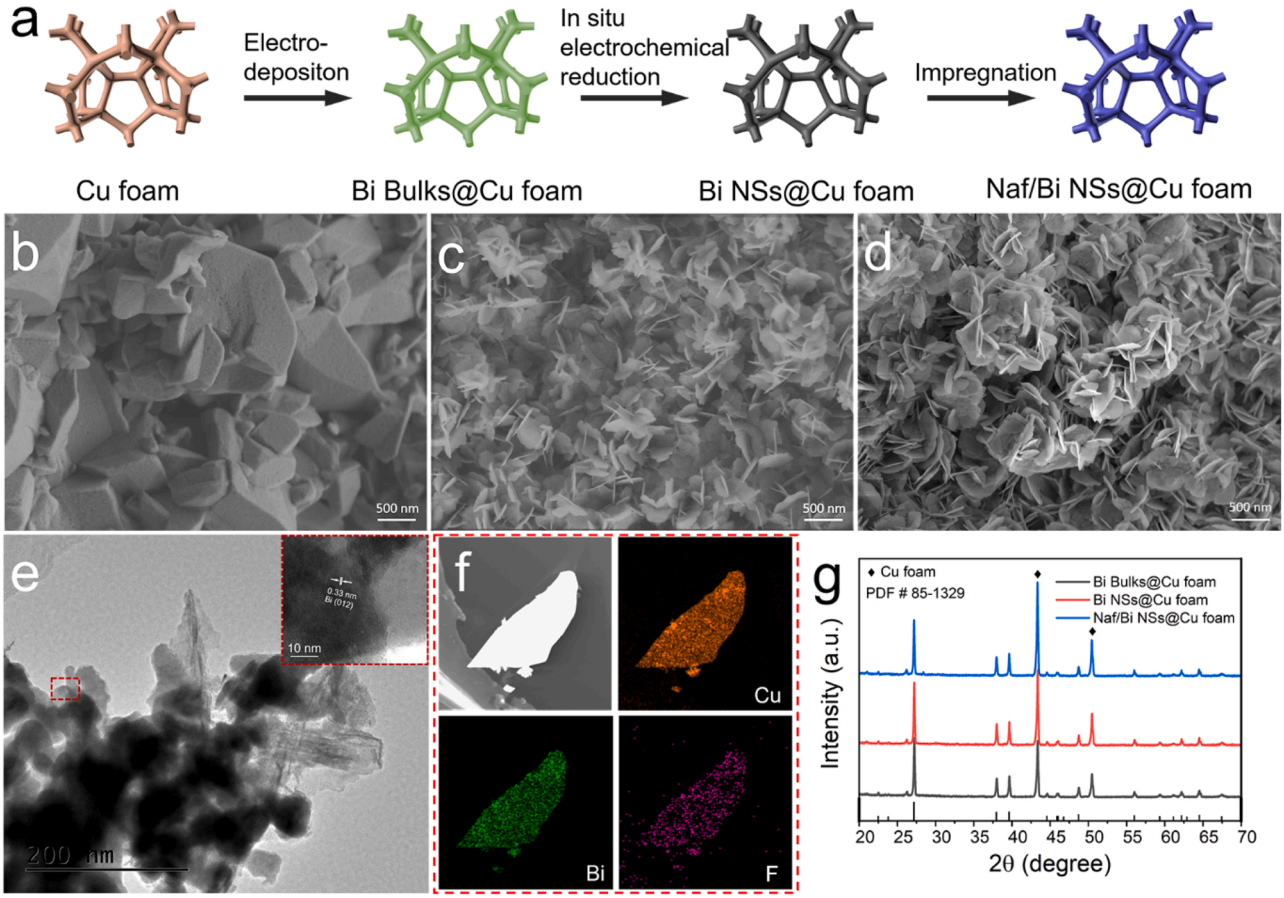

Fig. 1. Synthesis scheme and characterization of Naf/Bi NSs@Cu foam. (a) Schematic scheme of Naf/Bi NSs@Cu foam. SEM image of (b) Bi Bulks@Cu foam, (c) Bi NSs@Cu foam, and (d) Naf/Bi NSs@Cu foam. (e) TEM image, inset is the corresponding High resolution-TEM and (f) TEM EDS mapping of Naf/Bi NSs@Cu foam. (g) XRD patterns.

saturated 0.5 M $KHCO_3$ electrolyte. As shown in Fig. 2a, only one liquid product of formate for CO_2 reduction was detected by the ^1H NMR spectrum (Fig. S9), along with a little amount of H_2 and CO (Fig. S10), but their distribution varies a lot depending on the catalytic electrode. Naf/Bi NSs@Cu foam exhibited the highest faradaic efficiency toward conversion into formate ($FE_{formate}$), above 95% in the whole range (−0.67 ~ −1.17 V *vs.* RHE) and maximum $FE_{formate}$ (97.3%) achieved at − 1.07 V *vs.* RHE. In comparison, Bi NSs@Cu foam electrode reached the highest $FE_{formate}$ value of 88.8% at − 0.97 V *vs.* RHE and decreased gradually at a more negative potential because of restricted CO_2 diffusion or enhanced HER process [28]. What's more, the product on Cu foam was mainly H_2, only small fraction formate of which the maximum yield is ~8% at − 1.17 V *vs.* RHE. Other substances did not be observed during the electrolysis process (Fig. S11), indicating that the contribution of Cu foam substrate to improved $FE_{formate}$ is negligible. To further confirm this result, the Bi NSs catalyst was fabricated on carbon felt (CF) used as a substrate to investigate the performance of CO_2RR. Bulk electrolysis results of Bi NSs@CF also showed similar $FE_{formate}$ distribution (Fig. S12). In addition, the beneficial effect of Nafion modification was further confirmed by voltammetric plots of the partial current density of formate ($J_{formate}$) plotted against potential (Fig. 2b). Naf/Bi NSs@Cu foam showed a much higher $J_{formate}$ than those of Bi NSs@Cu foam and Cu foam at all tested potentials. Notably, the $J_{formate}$ of Naf/Bi NSs@Cu foam reached 94.86 mA cm^{-2} at − 1.17 V *vs.* RHE, which is about 93 and 1.8 times higher than that of Cu foam (1.01 mA cm^{-2}) and Bi NSs@Cu foam (52.62 mA cm^{-2}), demonstrating a facilitated CO_2RR process due to the unobstructed CO_2 diffusion pathways [55].

Furthermore, Naf/Bi NSs@Cu foam showed a larger transient current density in contrast to the pristine electrode (Fig. S13). To clarify the source of the large current density, double layer capacitance was measured to estimate the relative electrochemical active surface area (ESCA, Fig. S14). The measured double-layer capacitance together with $J_{formate}$ and ESCA normalized $J_{formate}$ values were listed in Table S1. As indicated by the double-layer capacitance, the ESCA of Naf/Bi NSs@Cu foam was about 1.25 and 8.6 times that of Bi NSs@Cu foam and pure Cu foam, respectively. Note that the ESCA of Bi NSs@CF was close to that of Bi NSs@Cu foam. Therefore, a remarkably large number of the active site was exposed from Bi NSs. Further, it is clearly shown that the normalized $J_{formate}$ of Naf/Bi NSs@Cu foam at − 1.07 V *vs.* RHE, was roughly 15 and 1.3 times that of Cu foam and Bi NSs@Cu foam, respectively. This suggested that the increased current density associated with Naf/Bi NSs@Cu foam and Bi NSs@Cu foam was derived from its large ESCA because Cu foam provided more active sites exposure due to its 3D porous structure. Electrochemical impedance spectroscopy (EIS, Fig. S15) results revealed that Nafion modification could lower the charge-transfer resistance, implying a favored charge transfer during the CO_2RR process promoted by Nafion modification [56].

Fig. 2c demonstrated the steady-state current densities of the CO_2RR promoted by the Naf/Bi NSs@Cu foam at various potentials, the steady current densities were observed in all cases. Since the electrode's durability directly determines whether it is industrially promising, the Naf/Bi NSs@Cu foam was tested at − 0.97 V *vs.* RHE by Chronoamperometry for 20-hour and the $FE_{formate}$ was calculated. As shown in Fig. 2d, Naf/Bi NSs@Cu foam exhibited a steady-state current density of 43.2 mA cm^{-2} over 20-hour operation without any significant decline, $FE_{formate}$ was maintained above 95%. In addition, the morphology (Fig. S16) and XRD pattern (Fig. S17) did not change obviously. In contrast, the current density on the Bi NSs@Cu foam was remarkably with reduced accompanying the change in morphology after 20-hours of electrolysis (Fig. S18), implying that Naf/Bi NSs@Cu foam

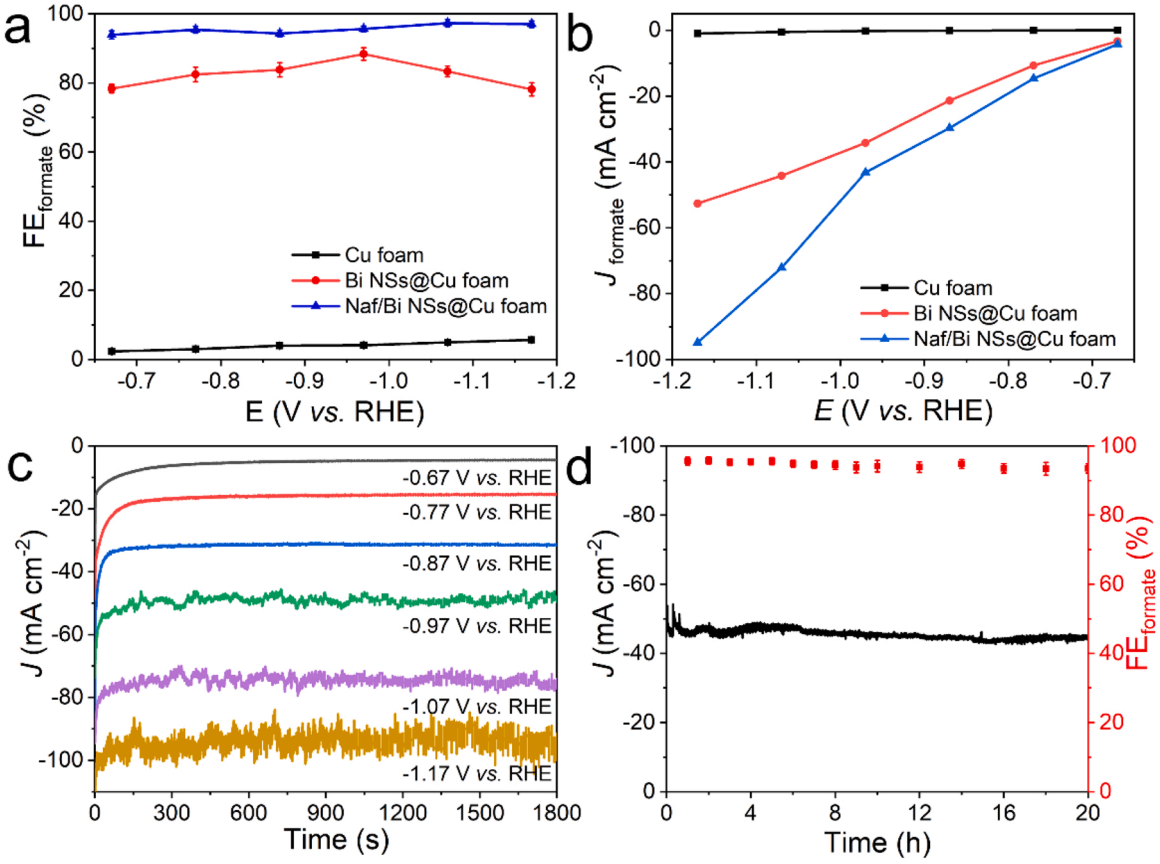

Fig. 2. (a) Faradaic efficiencies and (b) Partial current densities of formate on Cu foam, Bi NSs@Cu foam, and Naf/Bi NSs@Cu foam at a different potential. (c) Current densities of Naf/Bi NSs@Cu foam at various potentials in a CO_2-saturated 0.5 M $KHCO_3$. (d) Durability test of Naf/Bi NSs@Cu foam at the potential of − 0.97 V *vs.* RHE.

shows superior stability during the long-term electrolysis. Compared with the reported Bi-based catalysts for the CO_2RR in H-type cells, the as-synthesized Naf/Bi NSs@Cu foam showed outstanding superiority (Table S2). Significantly, the energy efficiency (EE, from electricity to formate product) of the CO_2RR with Naf/Bi NSs@Cu foam as the electrode was calculated, which is as high as 57% in a wide potential range (Fig. S19). Therefore, the Naf/Bi NSs@Cu foam shows great potential for CO_2RR into formate with high catalytic activity, selectivity, and stability. These results indicated that the Nafion modification will provide an effective method to optimize the CO_2RR performance.

3.3. CO_2RR enhancement at Bi/Nafion interface

Since Nafion as an overlayer was loaded on the Bi electrode surface, the local surrounding was divided into Nafion/electrolyte interface, Bi/Nafion, and Bi/electrolyte interface. The uniform nature of the Nafion overlayer according to aforementioned SEM and EDS mapping, (Fig. 1d, f, Fig. S7), suggested that the CO_2RR does not occur at the Bi/electrolyte interfaces like a non-uniform overlayer in which gaps in the Nafion layer would expose portions of this interface [49]. To demonstrate the CO_2RR occurs at the Bi/Nafion interface, we used different substrates to test the faradic efficiencies of the product and its partial current density at − 0.87 V *vs.* RHE. Two different substrates (Ni foam, Cu foam) as control experimental were tested without Nafion modification. As aforementioned test at − 0.87 V *vs.* RHE, Naf/Bi NSs@Cu foam showed a significantly enhanced $FE_{formate}$ of 88.8% while decreased FE_{H2}, compared with unmodified Bi NSs@Cu foam. As shown in Fig. 4a, b, unmodified Ni foam only produced H_2, while Nafion-modified Ni foam showed a significantly enhanced $FE_{formate}$ of 34.3% and a little CH_4 (2.3%). Compared with unmodified Cu foam, the Nafion-modified Cu foam demonstrated a decrease in H_2 production and an increase in formate production. Albeit the Nafion modification on different electrodes resulted in different product distribution, the hydrogen evolution reaction was greatly inhibited, while the performance of CO_2RR was significantly enhanced, especially the increased $FE_{formate}$. Notably, the Nafion-modified Ni foam only produces CH_4 in the same test condition. Because the product depends on the substrate and each substrate yields its own unique set of faradaic efficiency for each product. Therefore, we concluded that the CO_2RR to formate mainly occurs at the Bi NSs electrode and Nafion interface.

3.4. Origin of the improved CO_2RR performance

The CO_2RR to formate involves the PCET process, which has a significant effect on product selectivity at the Bi/Nafion interface [54,57] was speculated. To verify this hypothesis, the hydrophobic polymer poly (vinylidene fluoride) (PVDF) was used as an alternative to the Nafion, which could block proton transfer in the CO_2RR process [49]. PVDF modification on the electrode was conducted similarly with that of Nafion (Fig. 3c, d), which results in a great decrease $FE_{formate}$ on the PVDF modified electrode in the CO_2RR. As expected, the performance of Nafion modified electrode displayed a partial current density of 28.16 mA cm^{-2} and a $FE_{formate}$ of 88.8% at − 0.87 V *vs.* RHE, which was much better than the PVDF modified electrode with a partial current density of 15.97 mA cm^{-2} and a $FE_{formate}$ of 75.52%. These findings demonstrated that Nafion plays important role in the PCET process [49]. To explore the kinetics in the protonation for formate production, we carried out the performance of CO_2RR in electrolytes with different concentrations of HCO_3^- keeping the concentration of K^+ the same (1 M) by adding K_2SO_4 in the meantime, to avoid the influence of ion conductivity of electrolyte to the electrochemical reaction. The partial current densities used in the CO_2RR for producing formate as a function

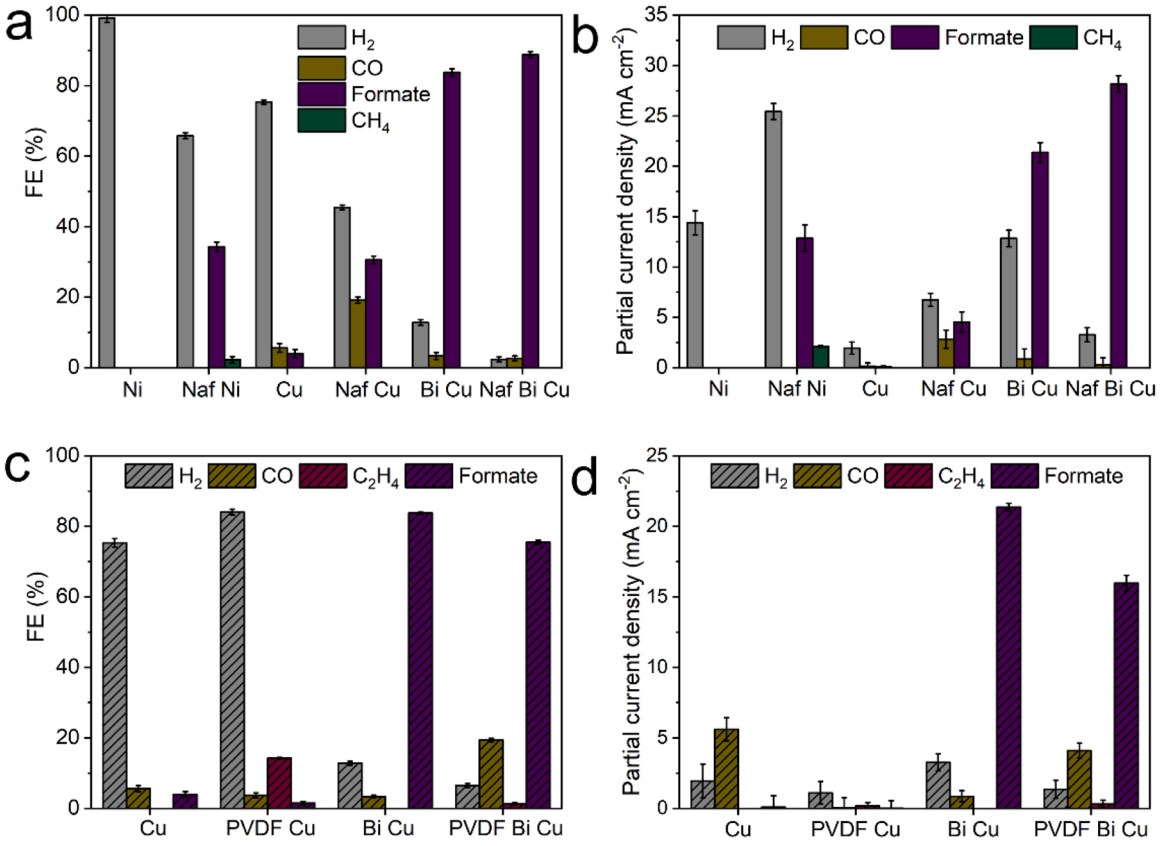

Fig. 3. (a) Faradic efficiencies, (b) partial current densities on the bare electrode (Ni foam (Ni), Cu foam (Cu), Bi NSs@Cu foam (Bi Cu))and Nafion-modified electrode (Naf Ni, Naf Cu, Naf Bi Cu), and (c) Faradic efficiencies, (b) partial current densities of different products on Bi NSs@Cu foam (Bi Cu) and PVDF-modified Bi NSs@Cu foam (PVDF Bi Cu) at − 0.87 V *vs.* RHE over 30 min in a CO_2-saturated 0.5 M $KHCO_3$.

of HCO_3^- concentration were presented in Fig. 4a. With the increase of the HCO_3^- concentration, $J_{formate}$ though Naf/Bi NSs@Cu foam (being tested −0.87 V *vs.* RHE) increases to the highest value of 34.8 mA cm^{-2} in 0.7 M CO_2-saturated $KHCO_3$ electrolyte, which is higher than that of Bi NSs@Cu foam (24.9 mA cm^{-2}). The study of Reaction-order further revealed that the $J_{formate}$ was nearly a quasi-first order dependency on HCO_3^- concentration (Fig. S20) [58]. Interestingly, the quasi-first order dynamic constants of Naf/Bi NSs@Cu foam and Bi NSs@Cu foam were almost uniform. On the other hand, Naf/Bi NSs@Cu foam exhibited higher $FE_{formate}$, lower FE_{H2} than Bi NSs@Cu foam over the entire range of HCO_3^- concentration (Fig. 4b). However, the $FE_{formate}$ and FE_{H2} did not increase with the increase of HCO_3^- concentration, which is consistent with quasi-first dynamics. Therefore, it is suggested that the Nafion enhances the local proton activity at the Bi/Nafion interface.

To investigate the source of protons for CO_2RR to formate, the isotope labeling experiment was conducted at a constant potential of − 0.87 V *vs.* RHE. As shown in Fig. 4c, the current density in the D_2O electrolyte was lower than that in H_2O. Furthermore, the $HCOO^-$ content in the total electrolyte produced at − 0.87 V *vs.* RHE was determined by ^1H NMR (Fig. 4d). The $HCOO^-$ relative content was 0.08/6 in H_2O electrolyte, much higher than 0.01/6 in D_2O, which demonstrated that protons to produce formate mainly come from HCO_3^-.

Nafion also promotes CO_2 adsorption at the Bi/Nafion interface. According to the previous discussion, it has been found that the electrochemical active surface area of Naf/Bi NSs@Cu foam was similar to that of the Bi NSs@Cu foam (Fig. S12, 14, Table S1), suggesting the active sites mainly originated from Bi NSs. Therefore, it can be concluded that the increased activity of CO_2RR results from Nafion modification onto the Bi electrode, which possibly facilitates the adsorption and activation of CO_2. In the CO_2RR process, the initial one-electron transfer to CO_2 for forming $*CO_2^-$ is generally believed to be the rate-determining step due to its highest activation energy [59,60], in which stabilization of the $*CO_2^-$ intermediate plays a crucial role. The binding affinity of $*CO_2^-$ onto as-prepared electrodes was identified using OH^- adsorption as a substitute, testified with cyclic voltammetry in N_2-saturated 0.1 M KOH electrolyte (Fig. S21). The result showed that the peak area of OH^- adsorption on the Nafion-modified electrode was larger than that of the Bi electrode, suggesting Nafion modification promotes CO_2 adsorption.

In the liquid electrolyte, the adsorption of CO_2 is closely related to the wettability of the electrode surface since the hydrophilic surface leads to electrolyte flooding and hinders the contact of CO_2 gases with reactive sites on the electrode surface [61]. Therefore, contact angle measurements were conducted to testify to the wettability of as-prepared electrodes. The contact angle of Bi NSs@Cu foam and Naf/Bi NSs@Cu foam are very close (140.3° and 142.4 °, Fig. S22). Interestingly, the contact angle of Bi NSs@Cu foam quickly declines to 9.0° after half-hour CO_2RR operation (Fig. S23a, b), further to 0.0° after 1 h, indicating Bi NSs@Cu foam can be easily flooded. As shown in Fig. S23c, d, the contact angle of Naf/Bi@Cu foam only decreases to 128 ° and 123 ° after 0.5-hour and 1-hour electrolysis, respectively. This suggested the Nafion modification maintains the electrodes' hydrophobicity and thus prevents it from electrolyte flooding, which leads to unimpeded CO_2 availability at the Bi/Nafion interface. This result demonstrated that CO_2 adsorption on the electrode surface is promoted due to the unrestricted diffusion of CO_2, which is consistent with the argument above-discussed.

The reconstruction of catalysts has been widely observed, which is triggered by negative potentials, electrolyte erosion, and so on. By modifying the electrode using Nafion, the reconstruction phenomenon

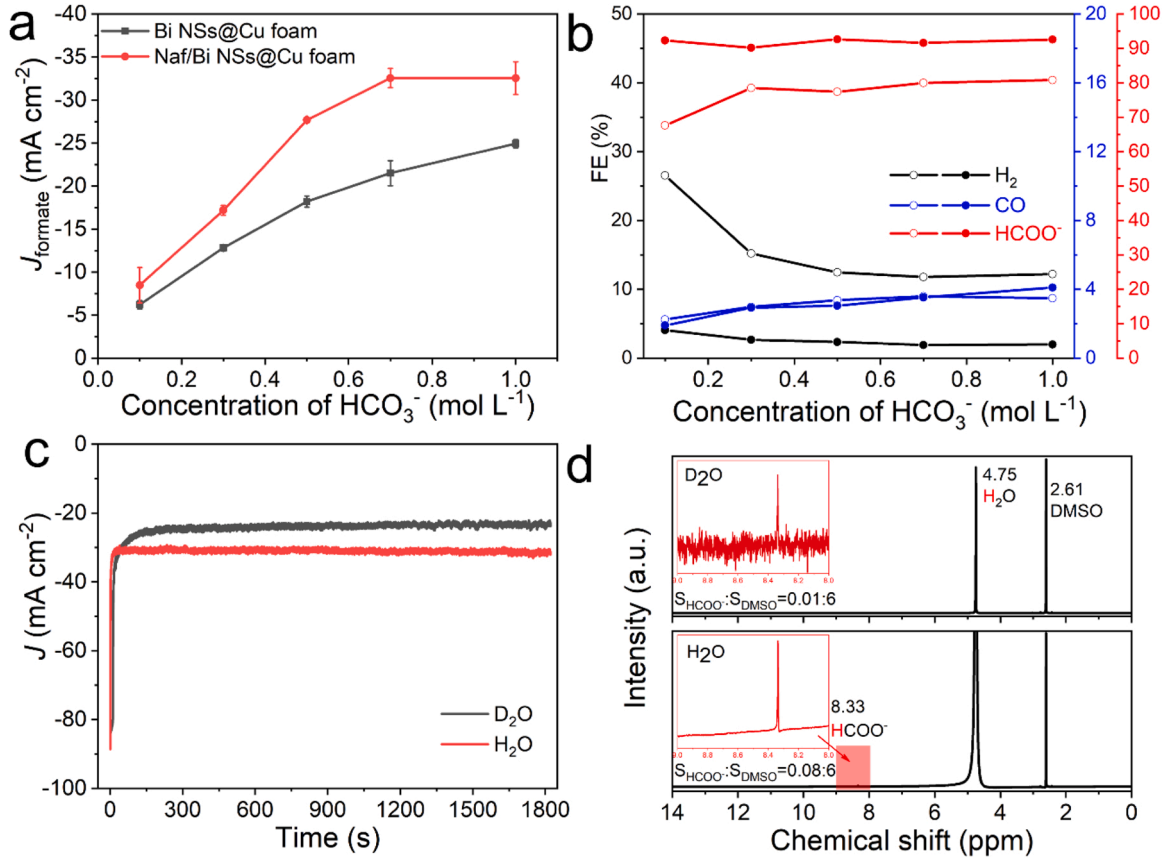

Fig. 4. (a) Partial current densities of formate and (b) Faradaic efficiencies on Bi NSs@Cu foam (hollow circle), and Naf/Bi NSs@Cu foam (solid circle) at − 0.87 V *vs.* RHE in different concentrated CO_2-saturated $KHCO_3$ electrolyte, where the total concentration of K^+ was kept 1 M by adding K_2SO_4. (c) Total current density, and (d) ^1H NMR spectra of the Naf/Bi NSs@Cu foam in CO_2-saturated 0.5 M $KHCO_3$ electrolyte under H_2O and D_2O conditions.

could be slowed down due to the adaptive Bi/Nafion interface environment, as verified by Operando electrochemical Raman testing of Bi NSs@Cu foam (Fig. 5a) and Naf/Bi NSs@Cu foam (Fig. 5b). At open circuit potential (OCP), Raman peaks near 68.7 cm^{-1} and 94.5 cm^{-1} correspond to the vibrational mode of Bi^0 of Bi NSs@Cu foam, while the peak at 158.5 cm^{-1} belongs to the Bi-O stretching mode of α-Bi_2O_3 (Fig. 5c) [30]. With applied potential changing from OCP to − 0.67 V *vs.* RHE, the intensity of Bi bands decreases, suggesting the catalyst reconstruction happens in the electrolysis process. Fig. 5d showed the Raman peaks of Naf/Bi NSs@Cu foam under OCP. Note that peak shifts were observed in Naf/Bi NSs@Cu foam compared with those of Bi NSs@Cu foam because of Nafion modification. As the applied potential changes, the intensity of the above characteristic peaks from Naf/Bi NSs@Cu foam remains stable (Fig. 5b), because Nafion acts as a protective layer to ensure the stability of the electrode surface during the electrolysis process. This result illustrated the importance of a stable interface for maintaining the stability of electrode structure.

3.5. Mechanism analysis

To obtain a deeper understanding of the enhanced performance of CO_2RR, the Gibbs free energies of each process during the CO_2RR at the Bi NSs surface with and without Nafion modification were calculated by Density Function Theory (DFT). The possible reaction pathway went through the formation of *OCHO intermediate, which was found to be the energetically favorable choice for formate production [62,63]. For the Bi interface (Fig. 4e), the rate-determine-step (RDS) of CO_2RR to formate is the second hydrogenation step from *OCHO to $*HCOO^-$ due to the large uphill energy (1.34 eV). While for the Nafion modified Bi interface (Naf/Bi), the RDS changes from the second hydrogenation step to the following $*HCOO^-$ desorption step with smaller uphill energy (0.75 eV). Therefore, Nafion modified Bi surface would stabilize *OCHO intermediate and enhance the selectivity for formate. Overall, Nafion modification could greatly promote the PECT process, resulting in the change of the rate-determining step from the second hydrogenation to the formate desorption process with a lower energy barrier (1.34 eV *vs*

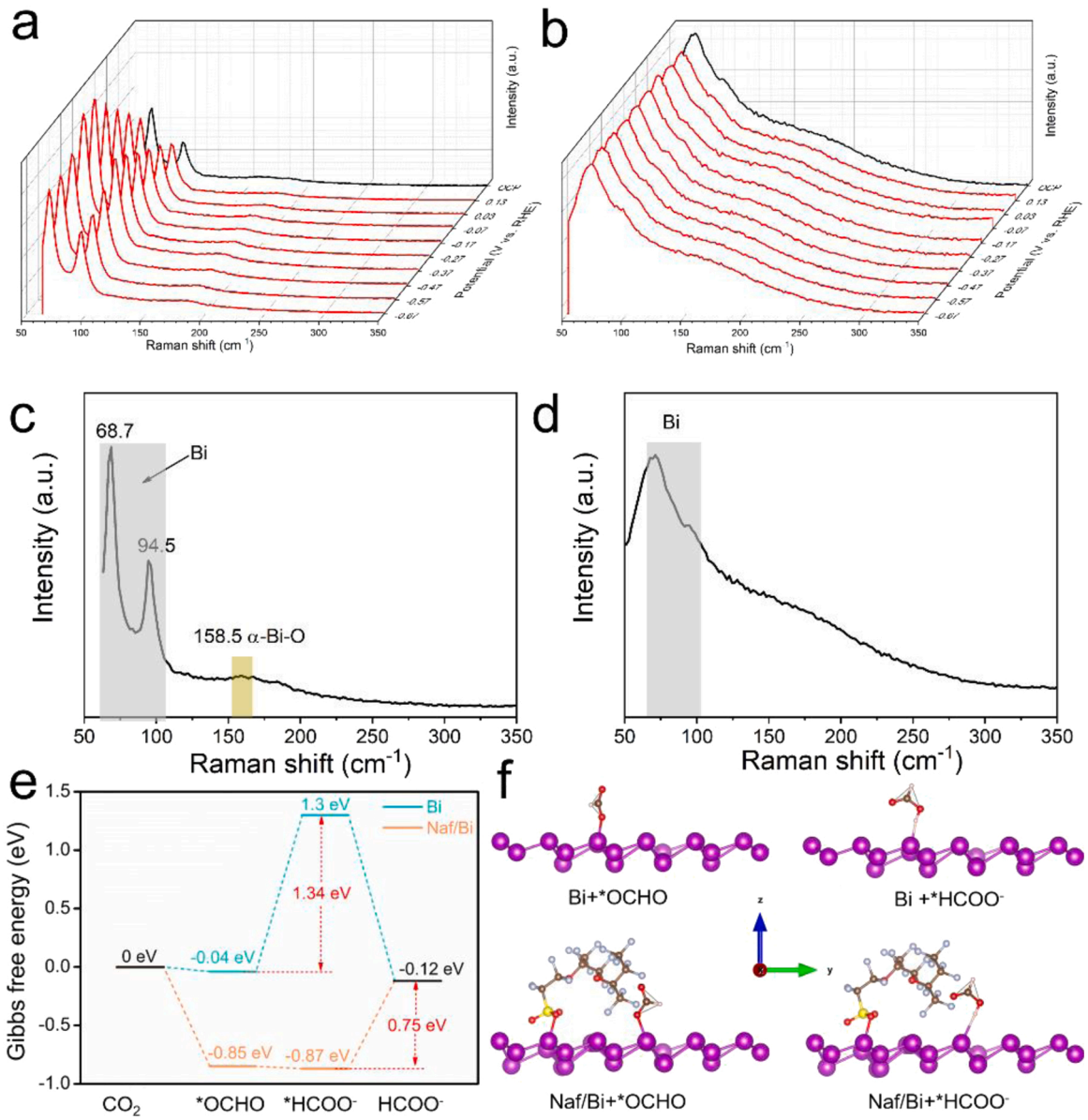

Fig. 5. *Operando* electrochemical Raman spectra of (a) Bi NSs@ Cu foam, and (b) Naf/Bi NSs@Cu foam at different applied potential, and (c, d) the Raman spectra under the open circuit potential extracted from (a, b), respectively. (e) Gibbs free energies of reaction pathways and (f) Configurations of corresponding reaction intermediates over Bi (Bi NSs@Cu foam) and Naf/Bi (Naf/Bi NSs@Cu foam).

0.75 eV). Based on the above results, the CO_2 reduction probably follows a reaction pathway of $*CO_2^-$→ *OCHO→ $*HCOO^-$. In the reaction process, we found that bicarbonates serve predominantly as a proton donor for *OCHO formation. Initially, the CO_2 molecular undergoes the first electron transfer step to form $*CO_2^-$. Then the subsequent protonation leads to the formation of $*OCHO^-$. Finally, $*HCOO^-$ is generated by the protonation of $*OCHO^-$ and then desorbs as formate from the electrode surface.

4. Conclusions

In summary, a strategy of a highly stable, active Bi/Nafion interface was proposed and realized by Nafion modification, which effectively improves the performance of CO_2RR to formate. The interface promotes the absorption and adsorption of CO_2, and then enhances local proton activity on the electrode surface, which enables formation of a high active reaction zone with the balance between CO_2 being reduced and protons being needed. We revealed that Nafion modification stabilizes the key intermediate *OCHO and greatly promotes the PECT process, resulting in transition of the rate-determining step from the second hydrogenation to the formate desorption process. Our work provides new insights into the local environment at the electrode interface, as well as a general approach to improve CO_2RR performance by interface engineering.

CRediT authorship contribution statement

Sheng Chang: Investigation, Data curation, Formal analysis, Methodology, Writing – original draft, Writing – review & editing. **Yimin Xuan:** Conceptualization, Methodology, Writing – review & editing, Project administration, Resources, Supervision, Validation. **Kai Zhang:** Formal analysis, Writing – review & editing. **Jingjing Duan:** Formal analysis, Writing – review & editing.

Declaration of Competing Interest

The authors declare that they have no known competing financial interests or personal relationships that could have appeared to influence the work reported in this paper.

Acknowledgments

The authors would like to acknowledge the financial support for this work from the Basic Science Center Program for Ordered Energy Conversion of the National Natural Science Foundation of China (NO. 51888103).

Appendix A. Supporting information

Supplementary data associated with this article can be found in the online version at doi:10.1016/j.apcatb.2022.121135.

References

[1] L. Zhang, Z. Zhao, J. Gong, Nanostructured materials for heterogeneous electrocatalytic CO_2 reduction and their related reaction mechanisms, Angew. Chem. Int. Ed. 56 (2017) 11326–11353.
[2] J. Jiao, R. Lin, S. Liu, W. Cheong, C. Zhang, Z. Chen, Y. Pan, J. Tang, K. Wu, S. Hung, H. Chen, L. Zheng, Q. Lu, X. Yang, B. Xu, H. Xiao, J. Li, D. Wang, Q. Peng, C. Chen, Y. Li, Copper atom-pair catalyst anchored on alloy nanowires for selective and efficient electrochemical reduction of CO_2, Nat. Chem. 11 (2019) 222–228.
[3] W. Ren, C. Zhao, Paths towards enhanced electrochemical CO_2 reduction, Natl. Sci. Rev. 7 (2020) 7–9.
[4] J. Qiao, Y. Liu, F. Hong, J. Zhang, A review of catalysts for the electroreduction of carbon dioxide to produce low-carbon fuels, Chem. Soc. Rev. 43 (2014) 631–675.
[5] S. Gao, Y. Lin, X. Jiao, Y. Sun, Q. Luo, W. Zhang, D. Li, J. Yang, Y. Xie, Partially oxidized atomic cobalt layers for carbon dioxide electroreduction to liquid fuel, Nature 529 (2016) 68–71.
[6] E.V. Kondratenko, G. Mul, J. Baltrusaitis, G.O. Larazabal, J. Perez-Raminrez, Status and perspectives of CO_2 conversion into fuels and chemicals by catalytic, photocatalytic and electrocatalytic processes, Energy Environ. Sci. 6 (2013) 3112–3135.
[7] R. Shi, J. Guo, X. Zhang, G.I.N. Waterhouse, Z. Han, Y. Zhao, L. Shang, C. Zhou, L. Jiang, T. Zhang, Efficient wettability-controlled electroreduction of CO_2 to CO at Au/C interface, Nat. Commun. 11 (2020) 3028.
[8] J.K. Pedersen, T.A.A. Batchelor, A. Bagger, J. Rossmeisl, High-entropy alloys as catalysts for the CO_2 and CO reduction reactions, ACS Catal. 10 (2020) 2169–2176.
[9] M. Liu, Y. Wang, H. Ding, M. Lu, G. Gao, L. Dong, Q. Li, Y. Chen, S. Li, Y. Lan, Self-assembly of anthraquinone covalent organic frameworks as 1D superstructures for highly efficient CO_2 electroreduction to CH_4, Sci. Bull. 66 (2021) 1659–1668.
[10] S. Chen, C. Zhu, H. Gu, L. Wang, J. Qi, L. Zhong, Z. Zhang, C. Yang, G. Shi, S. Zhao, S. Li, K. Liu, L. Zhang, Enhanced electrochemical methanation of carbon dioxide at the single-layer hexagonal Boron Nitride/Cu interfacial perimeter, Nano Lett. 21 (2021) 4469–4476.
[11] A. Ismail, G.F. Samu, H.C. Nguyen, E. Csapo, N. Lopez, C. Janaky, Au/Pb interface allows the methane formation pathway in carbon dioxide electroreduction, ACS Catal. 10 (2020) 5681–5690.
[12] J. Xie, J. Chen, Y. Huang, X. Zhang, W. Wang, G. Huang, H. Yu, Selective electrochemical CO_2 reduction on Cu-Pd heterostructure, Appl. Catal. B 270 (2020) 11864.
[13] Z. Wu, H. Wu, W. Cai, Z. Wen, B. Jia, L. Wang, W. Jin, T. Ma, Engineering Bismuth-Tin interface in Bimetallic Aerogel with a 3D porous structure for highly selective electrocatalytic CO_2 reduction to HCOOH, Angew. Chem. Int. Ed. 60 (2021) 12554–12559.
[14] P. Yue, Q. Fu, J. Li, L. Zhang, L. Xing, Z. Kang, Q. Liao, X. Zhu, Triple-phase electrocatalysis for the enhanced CO_2 reduction to HCOOH on a hydrophobic surface, Chem. Eng. J. 405 (2021), 126975.
[15] F. Li, G.H. Gu, C. Choi, P. Kolla, S. Hong, T.S. Wu, Y.L. Soo, J. Masa, S. Mukerjee, Y. S. Jung, J.S. Qiu, Z.Y. Sun, Highly stable two-dimensional bismuth metal-organic frameworks for efficient electrochemical reduction of CO_2, Appl. Catal. B 277 (2020), 119241.
[16] Q. Low, N.W.X. Loo, F. Calle-Vallejo, B. Yeo, Enhanced electroreduction of carbon dioxide to methanol using zinc dendrites pulse-deposited on silver foam, Angew. Chem. Int. Ed. 58 (2019) 2256–2260.
[17] Y. Wang, Z. Wang, C. Dinh, J. Li, A. Ozden, M.G. Kibria, A. Seifitokaldani, C. Tan, C.M. Gabardo, M. Luo, H. Zhou, F. Li, Y. Lum, C. Mccallum, Y. Xu, M. Liu, A. Proppe, A. Johnston, P. Todorovic, T. Zhuang, D. Sinton, S. Kelley, E. Sargent, Catalyst synthesis under CO_2 electroreduction favours faceting and promotes renewable fuels electrosynthesis, Nat. Catal. 3 (2020) 98–106.
[18] H. Liang, S. Zhao, X. Hu, M. Ceccato, T. Skrydstrup, K. Daasbjerg, Hydrophobic copper interfaces boost electroreduction of carbon dioxide to ethylene in water, ACS Catal. 11 (2021) 958–966.
[19] J. Zhang, J. Tang, L. Liu, J. Wang, The evolution of catalytically active calcium catalyst during steam gasification of lignite char, Carbon 172 (2021) 162–173.
[20] L. Rong, Z. Xu, J. Sun, G. Guo, New methyl formate synthesis method: coal to methyl formate, J. Energy Chem.. 27 (2018) 238–242.
[21] L. Zhu, Y. Liang, L. Sun, J. Wang, D. Xu, Highly efficient dehydrogenation of formic acid over binary palladium-phosphorous alloy nanoclusters on N-doped carbon, Inorg. Chem. 60 (2021) 10707–10714.
[22] L. Fan, C. Xia, P. Zhu, Y. Lu, H. Wang, Electrochemical CO_2 reduction to high-concentration pure formic acid solutions in an all-solid-state reactor, Nat. Commun.. 11 (2020) 3633.
[23] F. Li, L. Chen, G.P. Knowles, D.R. MacFarlane, J. Zhang, Hierarchical mesoporous SnO_2 nanosheets on carbon cloth: a robust and flexible electrocatalyst for CO_2 reduction with high efficiency and selectivity, Angew. Chem. Int. Ed. 56 (2017) 505–509.
[24] A.S. Agarwal, Y. Zhai, D. Hill, N. Sridhar, The electrochemical reduction of carbon dioxide to formate/formic acid: Engineering and economic feasibility, ChemSusChem 4 (2011) 1301–1310.
[25] K. Fan, Y. Jia, Y. Ji, P. Kuang, B. Zhu, X. Liu, J. Yu, Curved surface boosts electrochemical CO_2 reduction to formate via bismuth nanotubes in a wide potential window, ACS Catal. 10 (2020) 358–364.
[26] K. Ye, A. Cao, J. Shao, G. Wang, R. Si, N. Ta, J. Xiao, G. Wang, Synergy effects on Sn-Cu alloy catalyst for efficient CO_2 electroreduction to formate with high mass activity, Sci. Bull. 65 (2020) 711–719.
[27] G. Gong, P. Ding, M. Xu, X. Zhu, M. Wang, J. Deng, Q. Ma, N. Han, Y. Zhu, J. Lu, Structural defects on converted bismuth oxide nanotubes enable highly active electrocatalysis of carbon dioxide reduction, Nat. Commun. 10 (2019) 2807.
[28] X. Zhang, X. Sun, S. Guo, A.M. Bond, J. Zhang, Formation of lattice-dislocated bismuth nanowires on copper foam for enhanced electrocatalytic CO_2 reduction at low overpotential, Energy Environ. Sci. 12 (2019) 1334–1340.
[29] W. Zhang, Y. Hu, L. Ma, G. Zhu, Y. Wang, X. Xue, R. Chen, S. Yang, Z. Jin, Progress and perspective of electrocatalytic CO_2 reduction for renewable carbonaceous fuels and chemicals, Adv. Sci. 5 (2018), 1700275.
[30] Y. Zhao, X. Liu, Z. Liu, X. Lin, J. Lan, Y. Zhang, Y. Lu, M. Peng, T. Chan, Y. Tan, Spontaneously Sn-doped Bi/BiO_x core-shell nanowires toward high-performance CO_2 electroreduction to liquid fuel, Nano Lett. 21 (2021) 6907–6913.
[31] Y. Wang, R. Yang, Y. Chen, G. Gao, Y. Wang, S. Li, Y. Lan, Chloroplast-like porous bismuth-based core-shell structure for high energy efficiency CO_2 electroreduction, Sci. Bull. 65 (2020) 1635–1642.
[32] Y. Xing, X. Kong, X. Guo, Y. Liu, Q. Li, Y. Zhang, Y. Sheng, X. Yang, Z. Geng, J. Zeng, Bi@Sn core-shell structure with compressive strain boosts the electroreduction of CO(2) into formic acid, Adv. Sci. 7 (2020), 1902989.

[33] H. Xie, T. Zhang, R. Xie, Z. Hou, X. Ji, Y. Pang, S. Chen, M.M. Titirici, H. Weng, G. L. Chai, Facet engineering to regulate surface states of topological crystalline insulator bismuth rhombic dodecahedrons for highly energy efficient electrochemical CO_2 reduction, Adv. Mater. 33 (2021), 2008373.
[34] C. Gao, D. Ma, J. Gu, Y. Xie, G. Zeng, X. Li, S. Han, Q. Zhu, X. Wu, Q. Xu, Metal-organic layers leading to atomically thin bismuthene for efficient carbon dioxide electroreduction to liquid fuel, Angew. Chem. Int. Ed. 59 (2020) 15014–15020.
[35] S. He, F. Ni, Y. Ji, L. Wang, Y. Wen, H. Bai, G. Liu, Y. Zhang, Y. Li, B. Zhang, The p-orbital delocalization of main-group metals to boost CO_2 electroreduction, Angew. Chem. Int. Ed. 57 (2018) 16114–16119.
[36] Z. Wang, C. Wang, Y. Hu, S. Yang, J. Yang, W. Chen, H. Zhou, F. Zhou, L. Wang, J. Du, Simultaneous diffusion of cation and anion to access N, S co-coordinated Bi-sites for enhanced CO_2 electroreduction, Nano Res. 14 (2021) 2790–2796.
[37] M. Zhao, Y. Gu, W. Gao, P. Cui, H. Tang, X. Wei, H. Zhu, G. Li, S. Yan, X. Zhang, Atom vacancies induced electron-rich surface of ultrathin Bi nanosheet for efficient electrochemical CO_2 reduction, Appl. Catal. B 266 (2020), 118625.
[38] D. Zhuo, Q. Chen, X. Zhao, Y. Jiang, J. Lu, Z. Xu, G. Guo, Ce-doped Bi based catalysts for highly efficient electroreduction of CO_2 to formate, J. Mater. Chem. C 9 (2021) 7900–7904.
[39] X. Chen, H. Chen, W. Zhou, Q. Zhang, Z. Yang, Z. Li, F. Yang, D. Wang, J. Ye, L. Liu, Boron dopant induced electron-rich bismuth for electrochemical CO_2 reduction with high solar energy conversion efficiency, Small 17 (2021), 2101128.
[40] L. Jia, M. Sun, J. Xu, X. Zhao, R. Zhou, B. Pan, L. Wang, N. Han, B. Huang, Y. Li, Phase-dependent electrocatalytic CO_2 reduction on Pd_3Bi nanocrystals, Angew. Chem. Int. Ed. 60 (2021) 21741–21745.
[41] L. Li, A. Ozden, S. Guo, F. Pelayo García de Arquer, C. Wang, M. Zhang, J. Zhang, H. Jiang, W. Wang, H. Dong, D. Sinton, E.H. Sargent, M. Zhong, Stable, active CO_2 reduction to formate via redox-modulated stabilization of active sites, Nat. Commun. 12 (2021) 5223.
[42] L. Peng, Y. Wang, Y. Wang, N. Xu, W. Lou, P. Liu, D. Cai, H. Huang, J. Qiao, Separated growth of Bi-Cu bimetallic electrocatalysts on defective copper foam for highly converting CO_2 to formate with alkaline anion-exchange membrane beyond $KHCO_3$ electrolyte, Appl. Catal. B 288 (2020), 120003.
[43] W. Zhang, C. Xu, Y. Hu, S. Yang, L. Ma, L. Wang, P. Zhao, C. Wang, J. Ma, Z. Jin, Electronic and geometric structure engineering of bicontinuous porous Ag-Cu nanoarchitectures for realizing selectivity-tunable electrochemical CO_2 reduction, Nano Energy 73 (2020), 104796.
[44] Y. Zhong, Y. Xu, J. Ma, C. Wang, S. Sheng, C. Cheng, M. Li, L. Han, L. Zhou, Z. Cai, Y. Kuang, Z. Liang, X. Sun, An artificial electrode/electrolyte interface for CO_2 electroreduction by cation surfactant self-assembly, Angew. Chem. Int. Ed. 59 (2020) 19095–19101.
[45] S. Garg, M. Li, A.Z. Weber, L. Ge, L. Li, V. Rudolph, G. Wang, T.E. Rufford, Advances and challenges in electrochemical CO_2 reduction processes: an engineering and design perspective looking beyond new catalyst materials, J. Mater. Chem. A 8 (2020) 1511–1544.
[46] Y. Tan, K. Lee, H. Song, J. Oh, Modulating local CO_2 concentration as a general strategy for enhancing C-C coupling in CO_2 electroreduction, Joule 4 (2020) 1104–1120.
[47] Z. Li, Y. Yang, Z. Yin, Z. Yin, X. Wei, X. Peng, K.J. Lyu, F. Wei, L. Xiao, G. Wang, H. D. Abruna, J. Lu, L. Zhuang, Interface-enhanced catalytic selectivity on the C-2 products of CO_2 electroreduction, ACS Catal. 11 (2021) 2473–2482.
[48] Z. Xing, L. Hu, D.S. Ripatti, X. Hu, X. Feng, Enhancing carbon dioxide gas-diffusion electrolysis by creating a hydrophobic catalyst microenvironment, Nat. Commun. 12 (2021) 1–11.
[49] H. Pan, C.J. Barile, Electrochemical CO_2 reduction to methane with remarkably high faradaic efficiency in the presence of a proton permeable membrane, Energy Environ. Sci. 13 (2020) 3567–3578.
[50] S. A. Lee, J.W. Yang, S. Choi, H.W. Jang, Nanoscale electrodeposition: dimension control and 3D conformality, Exploration ⟨https://doi.org/10.1002/EXP.20210012⟩.
[51] J.P. Perdew, K. Burke, M. Ernzerhof, Generalized gradient approximation made simple, Phys. Rev. Lett. 77 (1996) 3865–3868.
[52] H.J. Monkhorst, J.D. Pack, Special points for brillouin-zone intergrations, Phys. Rev. B 13 (1976) 5188–5192, 5-88-5192.
[53] P. Hofmann, The surface of bismuth structural and electronic properties, Prog. Surf. Sci. 80 (2006) 191–245.
[54] M. Vijayakumar, M.S. Bhuvaneswari, P. Nachimuthu, B. Schwenzer, S. Kim, Z. Yang, J. Liu, G.L. Graff, S. Thevuthasan, J. Hu, Spectroscopic investigations of the fouling process on Nafion membranes in vanadium redox flow batteries, J. Membr. Sci. 366 (2011) 325–334.
[55] J.E. Pander, M.F. Baruch, A.B. Bocarsly, Probing the mechanism of aqueous CO_2 reduction on post-transition-metal electrodes using ATR-IR spectroelectrochemistry, ACS Catal. 6 (2016) 7824–7833.
[56] A.R.C. Bredar, A.L. Chown, A.R. Burton, Electrochemical impedance spectroscopy of metal oxide electrode for energy applications, ACS Appl. Energy Mater. 3 (2020) 66–98.
[57] M.B. Karimi, F. Mohammadi, K. Hooshyari, Recent approaches to improve Nafion performance for fuel cell applications: a review, Int. J. Hydrog. Energy 44 (2019) 28919–28938.
[58] X. Feng, K. Jiang, S. Fan, M.W. Kanan, Grain-boundary dependent CO_2 electroreduction activity, J. Am. Chem. Soc. 137 (2015) 4606–4609.
[59] S. Zhang, P. Kang, S. Ubnoske, M. Brennaman, N. Song, R.L. House, J.T. Glass, T. J. Meyer, Polyethylenimine-enhanced electrocatalytic reduction of CO_2 to formate at nitrogen-doped carbon nanomaterials, J. Am. Chem. Soc. 136 (2014) 7845–7848.
[60] F. Lei, Y. Sun, J. Xu, K. Liu, T. Yao, B. Pan, S. Wei, Y. Xie, Metallic tin quantum sheets confined in graphene toward high-efficiency carbon dioxide electroreduction, Nat. Commun. 7 (2016) 12697.
[61] Z. Xing, X. Hu, X. Feng, Tuning the microenvironment in gas-diffusion electrodes enables high-rate CO_2 electrolysis to formate, ACS Energy Lett. 6 (2021) 1694–1702.
[62] W. Zhang, S. Yang, M. Jiang, Y. Hu, C. Hu, X. Zhang, Z. Jin, Nanocapillarity and nanoconfinement effects of pipet-like Bismuth@Carbon nanotubes for highly efficient electrocatalytic CO_2 reduction, Nano Lett. 21 (2021) 2650–2657.
[63] W. Zhang, Y. Hu, L. Ma, G. Zhu, P. Zhao, X. Xue, R. Chen, S. Yang, J. Ma, J. Liu, Z. Jin, Liquid-phase exfoliated ultrathin bi nanosheets: uncovering the origins of enhanced electrocatalytic CO_2 reduction on two-dimensional metal nanostructure, Nano Energy 53 (2018) 808–816.